Quantitative Design and Evaluation of Enhancement/Thresholding Edge Detectors

IKRAM E. ABDOU AND WILLIAM K. PRATT, SENIOR MEMBER, IEEE

Abstract—Quantitative design and performance evaluation techniques are developed for the enhancement/thresholding class of image edge detectors. The design techniques are based on statistical detection theory and deterministic pattern-recognition classification procedures. The performance evaluation methods developed include: a) deterministic measurement of the edge gradient amplitude; b) comparison of the probabilities of correct and false edge detection; and c) figure of merit computation. The design techniques developed are used to optimally design a variety of small and large mask edge detectors. Theoretical and experimental comparisons of edge detectors are presented.

I. Introduction

EDGES are primitive features of an image that are widely used in image classification and analysis systems to outline the boundaries of objects. An image edge, as defined here, is a local change or discontinuity in image luminance.

There are two basic approaches to image edge detection: the enhancement/thresholding method and the edge fitting method. In the former, discontinuities in an image attribute are enhanced or accentuated by some spatial operator. If the enhanced discontinuity is sufficiently large—greater than some threshold level—an edge is deemed present. The edge fitting approach involves fitting of an ideal edge replica, a two-dimensional ramp or step function, to the image over some region. If the fit is close, an edge is judged present.

Although there is abundant literature [1, p. 478] on the subject of edge detection; the topic has not yet been covered in a unified, quantitative manner. This paper presents quantitative techniques for the design and evaluation of edge detectors based on the enhancement/thresholding method. A companion paper, in preparation, will consider the design and evaluation of edge fitting edge detectors.

II. Enhancement/Thresholding Luminance Edge Detectors

For the purpose of edge detector design and analysis, it is convenient to define an idealized luminance edge, illustrated in Fig. 1, as a planar ramp discontinuity. The ideal edge can be described by its Cartesian pixel coordinate (j, k), orientation

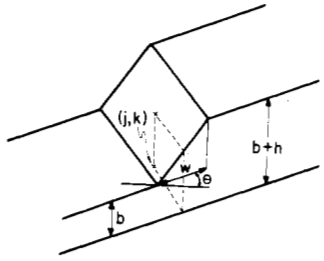

Fig. 1. Edge model.

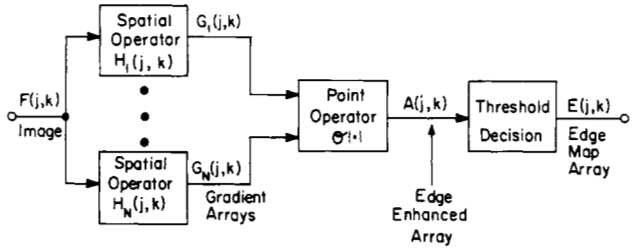

Fig. 2. Edge enhancement /thresholding edge detection system.

angle (θ), base amplitude (b), contrast (h), and slope width (w).

The edge enhancement/thresholding edge detection method is described in Fig. 2. In this method, the discrete image array $F(j, k)$ is spatially processed by a set of N linear operators or masks $H_i(j, k)$ to produce a set of gradient functions

$$G_i(j, k) = F(j, k) \circledast H_i(j, k) \tag{1}$$

where $\circledast$ denotes two-dimensional spatial convolution. Next, at each pixel, the gradient functions are combined by a linear or nonlinear point operator $\mathcal{O}\{\cdot\}$ to create an edge enhanced array

$$A(j, k) = \mathcal{O}\{G_i(j, k)\}. \tag{2}$$

Typical forms of the point operator include the root mean square (rms), magnitude, and maximum. The enhanced array $A(j, k)$ provides a measure of the edge discontinuity at the center of the gradient mask. An edge decision is formed on the basis of the amplitude of $A(j, k)$ with respect to a threshold (t). If

$$A(j, k) \geq t \tag{3a}$$

Manuscript received August 25, 1978; November 28, 1978. This work was supported by the Advanced Research Projects Agency of the Department of Defense and was monitored by the Wright-Patterson Air Force Base under Contract F-33615-76-C-1203.

I. E. Abdou was with the Image Processing Institute, University of Southern California, Los Angeles, CA. He is now with IBM Research Laboratory, San Jose, CA.

W. K. Pratt is with the Image Processing Institute, University of Southern California, Los Angeles, CA 90007.

0018-9219/79/0500-0753$00.75

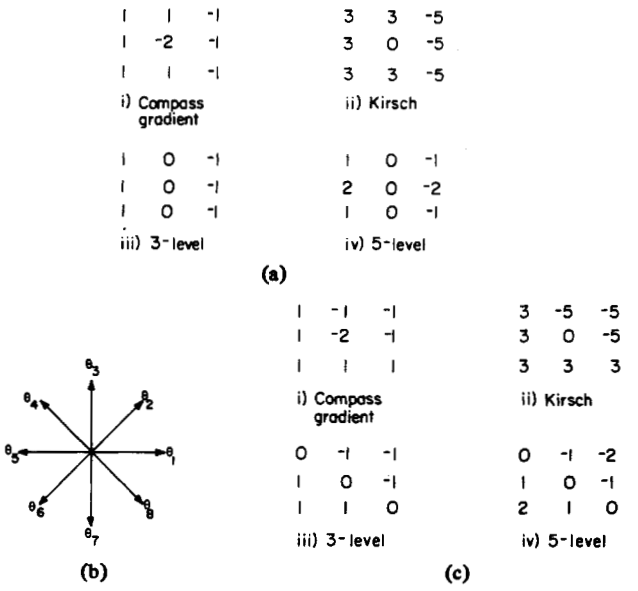

Fig. 3. Template matching operators. (a) Compass directions. (b) Mask H_1. (c) Mask H_2.

an edge is assumed present, and if

$$A(j, k) < t \tag{3b}$$

no edge is indicated. The edge decision is usually recorded as a binary edge map $E(j, k)$ where a one value indicates an edge and a zero value, no edge.

There are two types of spatial edge enhancement operators: the differential and the template matching operators. The following subsections present examples of each type of operator.

A. Differential Operators

The differential operators perform discrete differentiation of an image array to produce a gradient field. This group includes the Roberts [2], Prewitt [3], and Sobel [4, p. 271] operators. The Roberts operator is a 2 X 2 pixel mask in which[1]

$$H_1 = \begin{bmatrix} 0 & -1 \\ 1 & 0 \end{bmatrix} \tag{4a}$$

$$H_2 = \begin{bmatrix} -1 & 0 \\ 0 & 1 \end{bmatrix}. \tag{4b}$$

The Prewitt and Sobel operators are 3 X 3 pixel operators where

$$H_1 = \begin{bmatrix} 1 & 0 & -1 \\ c & 0 & -c \\ 1 & 0 & -1 \end{bmatrix} \tag{5a}$$

$$H_2 = \begin{bmatrix} -1 & -c & -1 \\ 0 & 0 & 0 \\ 1 & c & 1 \end{bmatrix}. \tag{5b}$$

With the Prewitt operator, $c = 1$ and with the Sobel operator, $c = 2$. These operators usually utilize an rms point nonlinearity to produce an edge enhanced array

$$A(j, k) = ([G_1(j, k)]^2 + [G_2(j, k)]^2)^{1/2}. \tag{6a}$$

[1] Note that the masks are rotated by 180° to compensate for the 180° rotation inherent to the convolution operation.

A magnitude point nonlinearity yielding

$$A(j, k) = |G_1(j, k)| + |G_2(j, k)| \tag{6b}$$

is often used for computational simplicity.

Edge orientation can be obtained from the relationship between the horizontal and vertical gradient functions. For the 2 X 2 operators, the edge orientation angle $\theta(j, k)$ with respect to the horizontal axis is defined to be

$$\theta(j, k) = \frac{\pi}{4} + \tan^{-1}\left[\frac{G_2(j, k)}{G_1(j, k)}\right] \tag{7a}$$

and for 3 X 3 operators

$$\theta(j, k) = \tan^{-1}\left[\frac{G_2(j, k)}{G_1(j, k)}\right]. \tag{7b}$$

B. Template Matching Operators

The template matching operators are a set of masks representing discrete approximations to ideal edges of various orientation. Fig. 3 gives several examples for two of eight possible compass orientations. These operators include the compass gradient introduced by Prewitt [3], the Kirsch [5], and the 3- and 5-level template masks. The latter two operators are related to the Prewitt and Sobel differential operators, respectively. With these operators, the enhancement is formed as the maximum of the gradient arrays. Thus

$$A(j, k) = \max_i \{|G_i(j, k)|\}. \tag{8}$$

The edge orientation $\theta(j, k)$ corresponds to the compass direction of the largest gradient. For the 3-level and 5-level operators, the outputs $G_i(j, k)$ of the first four masks suffice to specify the eight possible edge orientations.

C. Discussion

The specific edge detectors introduced above are widely used types of small mask detectors. Many other enhancement/thresholding edge detectors employing different, often larger,

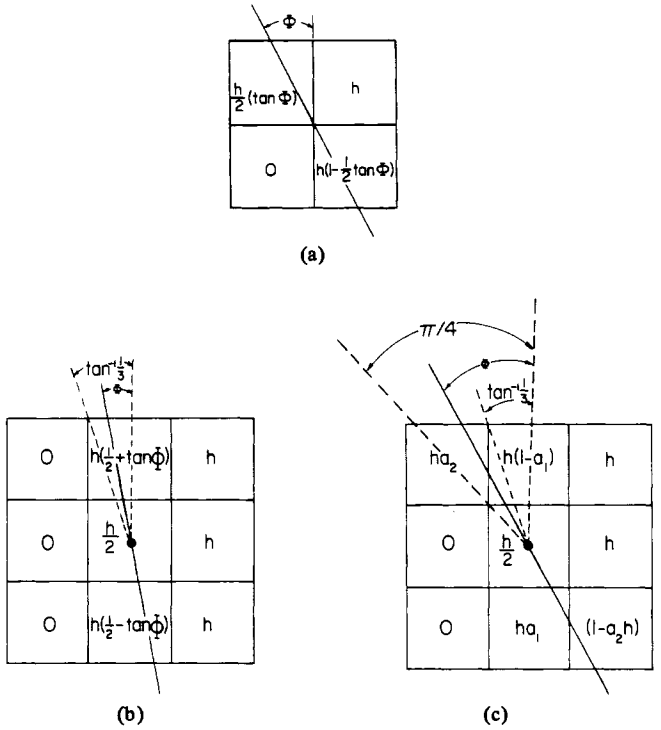

Fig. 4. Edge models for edge orientation sensitivity analysis:

$$a_1 = \frac{(1 - \tan\phi)^2}{8 \tan\phi} \qquad a_2 = \frac{(3 \tan\phi - 1)^2}{8 \tan\phi}$$

(a) 2 X 2 model. (b) 3 X 3 model, $0 \leqslant \phi \leqslant \tan^{-1}(1/3)$ (c) 3 X 3 model, $\tan^{-1}(1/3) < \phi \leqslant \pi/4$

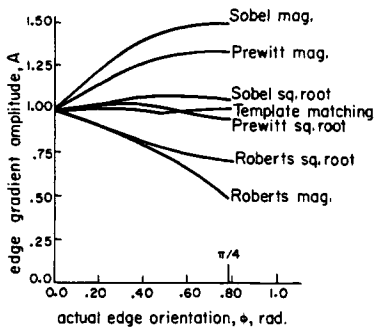

Fig. 5. Edge gradient amplitude response as a function of actual edge orientation for 2 X 2 and 3 X 3 operators.

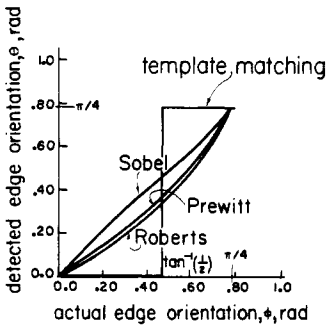

Fig. 6. Detected edge orientation as a function of actual edge orientation for 2 X 2 and 3 X 3 operators.

mask functions have been proposed. Analysis and comparison of these mask functions is deferred to Section VII. The intervening sections describe design and evaluation methods using the edge detectors introduced in this section as examples.

III. Edge Detector Sensitivity Analysis

Desirable properties of any edge detector are an amplitude response invariance to edge orientation and a lack of bias in orientation measurement. Edge detector sensitivity is considered here for ideal, noise-free edges. The effect of noise is covered in the following sections.

Fig. 4 contains models of ideal step edges passing through enhancement masks. Pixel amplitudes under the mask vary as a function of edge orientation as a result of the inherent averaging associated with discretization of the sampled image array.

Simple geometric calculations can be performed to determine the edge gradient and detected edge orientation response as a function of actual edge orientation for the edge models of Fig. 4 [6]. Results of these calculations are presented in Figs. 5 and 6. In Fig. 5, the edge gradient response is normalized to unity for a vertical edge. The curves indicate that the Prewitt and Sobel square root differential operators and the template matching operators all possess an amplitude response relatively invariant to actual edge orientation. The Sobel operator provides the most linear response between actual and detected edge orientation.

Another desirable edge detector property is a rapidly declining edge gradient response as the detector mask moves away from a central edge. Fig. 7 contains edge models of vertical and diagonal edges displaced from the mask center. Geometric

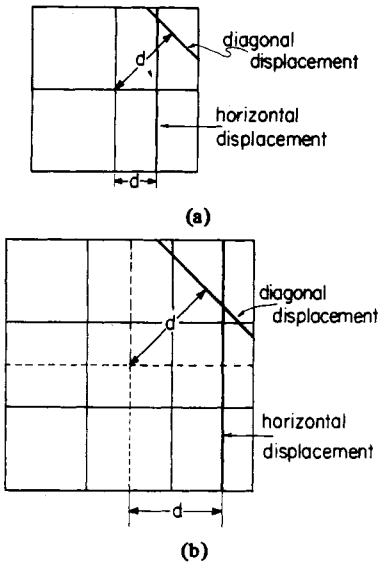

Fig. 7. Edge models for edge displacement sensitivity analysis. (a) 2 X 2 model. (b) 3 X 3 model.

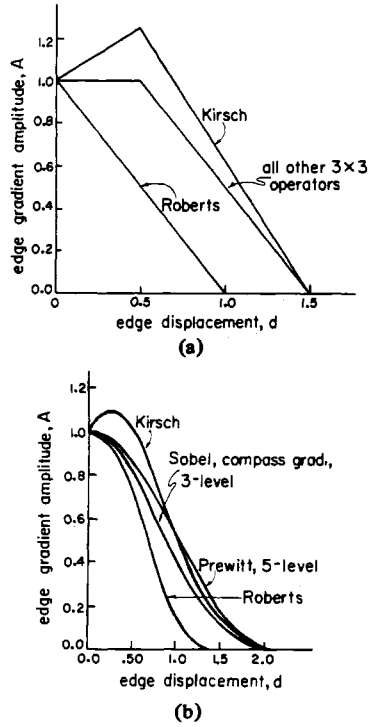

Fig. 8. Edge gradient amplitude response as a function of edge displacement for 2 X 2 and 3 X 3 operators. (a) vertical edge. (b) diagonal edge.

calculations yield a relationship between the edge detector amplitude response and displacement distance. Fig. 8 contains plots of the displacement sensitivity. All of the operators, with the exception of the Kirsch operator, exhibit a desired monotonically decreasing response as a function of edge displacement.

IV. Statistical Design Procedure

The threshold value (t) on an enhancement/thresholding type of edge detector controls the sensitivity of the edge detector. For noise-free images, the threshold can be chosen such that all discontinuities of a minimum contrast level are detected as edges, and all others are called no-edges. With noisy images, however, threshold selection becomes a tradeoff between the missing of valid edges and the creation of noise-induced false edges. This section considers a statistical design procedure for threshold selection. A deterministic approach is discussed in the following section.

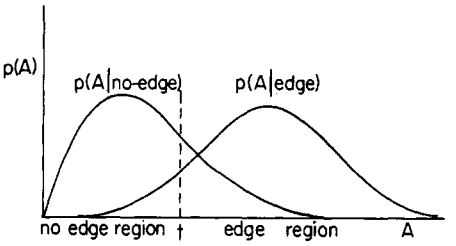

Fig. 9. Typical conditional probability density functions of edge enhancement.

Edge detection can be regarded as a hypothesis testing problem to determine if an image region contains an edge or contains no edge. Let P (edge) and P (no-edge) denote the *a priori* probabilities of these events. Then, the edge detection process can be characterized by the probability of correct edge detection

$$P_D = P(A \geq t \,|\, \text{edge}) = \int_t^\infty p(A \,|\, \text{edge})\, dA \tag{9}$$

and the probability of false edge detection

$$P_F = P(A \geq t \,|\, \text{no-edge}) = \int_t^\infty p(A \,|\, \text{no-edge})\, dA \tag{10}$$

where (t) is the edge decision threshold and $p(A|\text{edge})$ and $p(A|\text{no-edge})$ are the conditional probability densities of the edge enhanced field $A(j, k)$. Fig. 9 contains a sketch of typical densities. The probability of edge misclassification error can be expressed as

$$P(\text{error}) = [1 - P_D]\, P(\text{edge}) + [P_F]\, P(\text{no-edge}). \tag{11}$$

This error will be minimum if the threshold is chosen such that the edge hypothesis is accepted if

$$\frac{p(A \,|\, \text{edge})}{p(A \,|\, \text{no-edge})} \geq \frac{P(\text{no-edge})}{P(\text{edge})} \tag{12}$$

and the no-edge hypothesis is accepted otherwise. Equation (12) defines the well-known maximum likelihood ratio test associated with the Bayes minimum error decision rule of classical detection theory [7]. Decision strategies also exist for minimizing the cost-weighted error (Bayes minimum cost test), minimizing P_F for a fixed acceptable P_D (Neyman-Pearson test), and minimizing the maximum possible error (minimax test) [7].

Application of a statistical decision rule to edge detection to determine the threshold value requires knowledge of the conditional densities of the edge enhanced image and the *a priori* edge probabilities. The a priori probabilities can be estimated from images of the class under analysis. Alternatively, the a priori probability ratio can be regarded as a sensitivity control factor for the edge detector. The conditional densities can be found in terms of a probability density model for the original image plus knowledge of the edge detector operator law. The

TABLE I
MEAN VECTOR AND COVARIANCE MATRIX OF DIFFERENTIAL GRADIENT OPERATORS

Operator	η_g No-Edge	η_g Vertical Edge	η_g Diagonal Edge	K_g
Roberts	$\begin{bmatrix}0\\0\end{bmatrix}$	$\begin{bmatrix}1\\-1\end{bmatrix}$ h	$\begin{bmatrix}1\\0\end{bmatrix}$ h	$\begin{bmatrix}\sqrt{2} & 0\\ 0 & \sqrt{2}\end{bmatrix}\sigma$
Sobel	$\begin{bmatrix}0\\0\end{bmatrix}$	$\begin{bmatrix}4\\0\end{bmatrix}$ h	$\begin{bmatrix}3\\3\end{bmatrix}$ h	$\begin{bmatrix}\sqrt{12} & 0\\ 0 & \sqrt{12}\end{bmatrix}\sigma$
Prewitt	$\begin{bmatrix}0\\0\end{bmatrix}$	$\begin{bmatrix}3\\0\end{bmatrix}$ h	$\begin{bmatrix}2\\2\end{bmatrix}$ h	$\begin{bmatrix}\sqrt{6} & 0\\ 0 & \sqrt{6}\end{bmatrix}\sigma$

common case of additive, independent, white Gaussian noise will be given as an example of the design technique.

Let f be a $Q \times 1$ vector of pixel amplitudes lying under an edge detector mask ($Q = 9$ for a 3×3 mask). Vector f is assumed to be composed of samples of an ideal edge region s plus a Gaussian noise component n of zero mean and common variance σ^2. Thus

$$f = s + n. \tag{13}$$

The probability density of f can be written in general form as

$$p(f) = \mathcal{G}(f, \eta_f, K_f) \equiv (2\pi)^{-Q/2} |K_f|^{-1/2} \exp\left\{-\tfrac{1}{2}(f-\eta_f)^T K_f^{-1} (f-\eta_f)\right\} \tag{14}$$

where η_f and K_f are the mean vector and covariance matrix of f, respectively. For the model under consideration, the noise is independent and the edge s is deterministic. Hence, η_f can be determined from the edge model and $K_f = \sigma^2 I$ where I is an identity matrix.

Since the gradient operation of the edge detector is linear, the gradient outputs $G_i(j, k)$ are Gaussian random variables. Let

$$g = \begin{bmatrix} G_1(j,k) \\ G_2(j,k) \\ \vdots \\ G_N(j,k) \end{bmatrix} \tag{15}$$

be the vector formed by each of the N gradient operators. Then,

$$p(g) = \mathcal{G}(g, \eta_g, K_g) \tag{16}$$

where

$$\eta_g(k) = \sum_{j=1}^{Q} M_k(j)\, s(j) \tag{17a}$$

$$K_g(k,l) = \sigma^2 \sum_{j=1}^{Q} M_k(j)\, M_l(j) \tag{17b}$$

TABLE II
MEAN VECTOR AND COVARIANCE MATRIX OF TEMPLATE MATCHING OPERATORS FOR A VERTICAL EDGE

Operator	η_g	K_g
3-Level	$\begin{bmatrix}3\\2\\0\\-2\\-3\\-2\\0\\2\end{bmatrix}$ h	$\begin{bmatrix}6&4&0&-4&-6&-4&0&4\\4&6&4&0&-4&-6&-4&0\\0&\cdot&&&&&\cdot&\\-4&&\cdot&&&&&\cdot\\-6&&&\cdot&&&&\\-4&&&&\cdot&&&\\0&\cdot&&&&&\cdot&\\4&&\cdot&&&&&\cdot\end{bmatrix}\sigma^2$
5-Level	$\begin{bmatrix}4\\3\\0\\-3\\-4\\-3\\0\\3\end{bmatrix}$ h	$\begin{bmatrix}12&8&0&-8&-12&-8&0&8\\8&12&8&0&-8&-12&-8&0\\0&\cdot&&&&&\cdot&\\-8&&\cdot&&&&&\cdot\\-12&&&\cdot&&&&\\-8&\cdot&&&&\cdot&&\\0&\cdot&&&&&\cdot&\\8&&\cdot&&&&&\cdot\end{bmatrix}\sigma^2$
Compass Gradient	$\begin{bmatrix}3\\2\\0\\-2\\-3\\-2\\0\\2\end{bmatrix}$ h	$\begin{bmatrix}12&8&4&0&0&0&4&8\\8&12&8&4&0&0&0&4\\4&\cdot&&&&&\cdot&\\0&&\cdot&&&&&\cdot\\0&&&\cdot&&&&\\0&&&&\cdot&&&\\4&\cdot&&&&&\cdot&\\8&&\cdot&&&&&\cdot\end{bmatrix}\sigma^2$
Kirsch	$\begin{bmatrix}12\\8\\0\\-8\\-12\\-8\\0\\8\end{bmatrix}$ h	$\begin{bmatrix}120&56&-8&-72&-72&-72&-8&56\\56&120&56&-8&-72&-72&-72&-8\\-8&\cdot&&&&&\cdot&\\-72&&\cdot&&&&&\cdot\\-72&&&\cdot&&&&\\-72&\cdot&&&&\cdot&&\\-8&\cdot&&&&&\cdot&\\56&&\cdot&&&&&\cdot\end{bmatrix}\sigma^2$

represent general terms of the mean and covariance matrices of g, respectively. In (17), $M_k(j)$ denotes the column scanned jth term of the kth convolution mask. To complete the analysis, it is necessary to examine specific edge detectors.

Tables I and II list mean vectors and covariance matrices of the two-component Roberts, Sobel, and Prewitt differential operators for vertical and diagonal edges and the eight-component template matching operators for a vertical edge. The conditional densities $p(A|\text{edge})$ and $p(A|\text{no-edge})$ and the corresponding detection probabilities have been derived [6] for the differential operators. In the case of the template matching operators, the conditional densities are difficult to

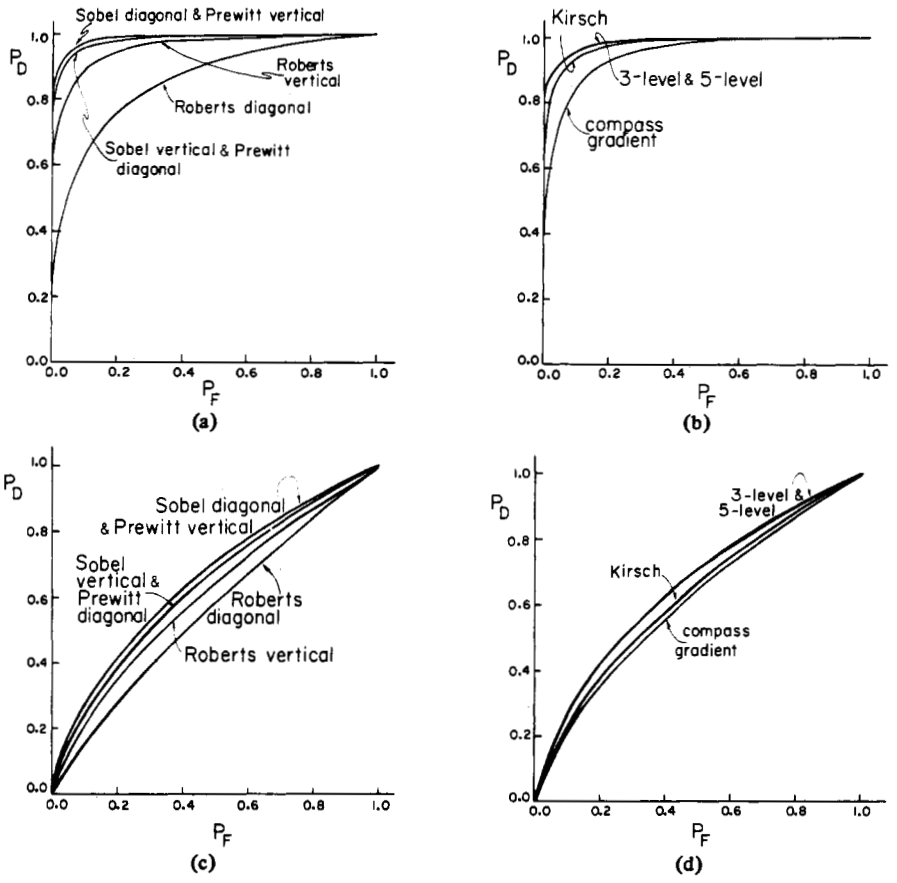

Fig. 10. Probability of detection versus probability of false detection for 2 X 2 and 3 X 3 operators. (a) Differential operators, SNR = 10. (b) Template operators, SNR = 10. (c) Differential operators, SNR = 1. (d) Template operators, SNR = 1.

state explicitly, but the error probabilities can be determined numerically.

The detection performance of edge detectors can be readily compared by a parametric plot of the correct detection probability P_D versus false detection probability P_F in terms of the detection threshold (t). Fig. 10 presents such plots for square root differential operators and template matching operators for vertical and diagonal edges and a signal-to-noise ratio[2] (SNR) of 1.0 and 10.0. From these curves, it is apparent that the Sobel and Prewitt 3 X 3 operators are superior to the Roberts 2 X 2 operators. The Prewitt operator is better than the Sobel operator for a vertical edge. But, for a diagonal edge, the Sobel operator is superior. In the case of template matching operators, the 3-level and 5-level operators exhibit almost identical performance superior to the Kirsch and compass gradient operators. Finally, the Sobel and Prewitt differential operators perform slightly better than the 3-level and 5-level template matching operators.

V. Pattern Classification Design Procedure

There are two difficulties with the statistical design procedure described in the previous section: reliability of the stochastic edge model and analytic problems associated with complex edge models such as non-Gaussian signal-dependent noise. The pattern classification design procedure described in this section avoids these difficulties.

Edge detection can be viewed as a classical pattern recognition or classification problem. A pattern consisting of the pixels encompassed by an edge detection operator is classified as a region containing an edge or no-edge on the basis of an extracted region feature, the amplitude $A(j, k)$ of the edge enhancement. Classification can be accomplished by the linear discriminant function method [8] in which the edge hypothesis is selected if

$$w^T x > 0 \tag{18a}$$

and rejected if

$$w^T x < 0 \tag{18b}$$

where $w(1)$ and $w(2)$ are weighting factors of the weight vector $w = [w(1), w(2)]^T$ and $x = [A, 1]^T$. The weight factors are related to the decision threshold by

$$t = -\frac{w(2)}{w(1)}. \tag{19}$$

Components of w can be determined by a training procedure using a set of prototype pixel regions containing edges or no-edges. Let $\{x_1, x_2, \cdots, x_M\}$ and $\{x_{M+1}, x_{M+2}, \cdots, x_{2M}\}$ represent sets of M edge and M no-edge prototypes, respectively. Then, equations (18a) and (18b) can be reformulated as a

[2] Signal-to-noise ratio is defined as SNR = $(h/\sigma)^2$ where h is the edge contrast and σ is the noise standard deviation.

TABLE III
THRESHOLD LEVEL AND ERROR PROBABILITIES FOR HO-KASHYAP DESIGN PROCEDURE

	Vertical Edge, SNR = 1					Vertical Edge, SNR = 10					Diagonal Edge, SNR = 1					Diagonal Edge, SNR = 10				
		experiment		theory			experiment		theory			experiment		theory			experiment		theory	
Operator	$\tilde{t}$	P_D	P_F	P_D	P_F	$\tilde{t}$	P_D	P_F	P_D	P_F	$\tilde{t}$	P_D	P_F	P_D	P_F	$\tilde{t}$	P_D	P_F	P_D	P_F
Roberts Square Root	1.36	52.0	37.6	55.89	39.87	0.67	91.2	11.6	89.16	10.47	1.74	55.60	46.80	55.10	46.88	0.78	74.80	20.80	77.79	22.11
Roberts Magnitude	1.22	52.0	38.4	55.16	39.30	0.62	90.8	7.6	89.20	9.85	2.24	54.40	46.40	53.85	45.70	0.97	75.60	19.60	76.81	23.30
Sobel Square Root	1.18	60.8	41.2	60.01	39.54	0.66	92.0	9.6	92.34	5.69	1.14	63.20	39.20	60.40	37.63	0.63	90.80	9.20	94.65	5.28
Prewitt Square Root	1.16	59.5	36.6	60.80	38.40	0.66	93.0	3.8	91.20	4.80	1.19	61.20	39.60	59.27	38.71	0.64	90.00	8.40	93.07	6.42
Compass Gradient	1.52	57.6	45.2	61.27	46.56	0.73	85.2	12.8	88.58	13.55	1.51	57.60	46.80	61.80	47.20	0.71	80.80	14.00	90.00	15.30
Kirsch	1.43	56.0	38.4	53.08	34.08	0.69	89.2	9.2	89.78	5.76	1.45	54.40	36.00	52.40	32.40	0.79	82.80	3.60	82.50	2.30
3-Level	1.16	60.8	38.4	59.02	36.92	0.65	89.6	6.4	92.64	3.79	1.16	59.20	38.40	58.70	36.50	0.61	89.60	8.40	94.60	5.60
5-Level	1.24	58.0	37.6	58.12	36.09	0.66	90.8	6.8	92.45	4.90	1.22	60.40	39.20	59.30	37.40	0.65	90.00	8.40	93.10	5.40

search for a vector w for which

$$X w > 0 \tag{20}$$

where

$$X = \begin{bmatrix} x_1 \\ \vdots \\ x_M \\ -x_{M+1} \\ \vdots \\ -x_{2M} \end{bmatrix}. \tag{21}$$

If there exists some w satisfying (20), then the prototype data is said to be linearly separable, otherwise it is linearly non-separable. In the latter case, a weight vector w is sought to minimize some misclassification error criterion function. One common choice is the mean-square misclassification distance

$$J(w) = (X w - b)^T (X w - b) \tag{22}$$

where $b \geqslant O$ is a vector of positive bias constants. In this study, the Ho-Kashyap algorithm [4, p. 151, 9] has been employed to find the optimum weight vector. Reasons for its selection and details of its applications to the edge detection design problem are found in reference [6].

An experiment has been performed to evaluate the pattern classification edge detector design procedure. In this experiment, sets of 20 edge prototypes and 20 no-edge prototypes have been generated for vertical and diagonal edges embedded in independent Gaussian noise at signal-to-noise ratios of 1.0 to 10.0. This prototype data has then been used to determine the optimum threshold. After the training phase was completed, the edge detectors were tested with 250 other prototypes. Optimum thresholds and detection probabilities are tabulated in Table III for various edge detectors. [3] It is interesting to note that in most cases the optimum threshold converged to a value for which the error probabilities were approximately equal ($P_F \approx 1 - P_D$). This is the same result that is obtained by the Bayes minimum error design procedure if edges and no edges are equally probable. Thus in the Gaussian noise case, similar design results are obtained with the statistical and pattern classification design approaches.

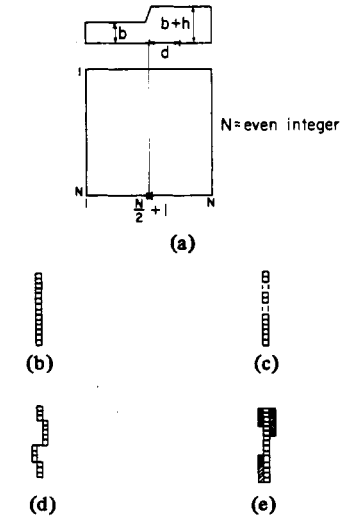

Fig. 11. Types of edge detection errors. (a) Vertical edge test image. (b) Ideal. (c) Fragmented. (d) Offset. (e) Smeared.

VI. FIGURE OF MERIT COMPARISON

The probabilities of correct detection and false detection, obtained analytically or experimentally, are useful performance indicators for edge detectors. However, these detection probability functions do not distinguish between the various types or errors than can be introduced by an edge detector as indicated in the example of Fig. 11. Fram and Deutsch [10], [11] have suggested an edge detector figure of merit based on a combination of experimentally measured correct and false detection probabilites. The simple mean-square distance figure of merit introduced by Pratt [1, p. 495] has been chosen here for evaluation of enhancement/thresholding edge detectors.

[3] For purposes of comparison, the decision threshold is normalized as $\tilde{t} = t/A_M$ where A_M denotes the maximum value of the edge enhancement in the absence of noise.

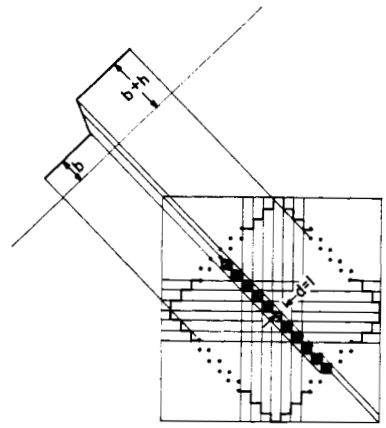

Fig. 12. Figure of merit test image geometry for diagonal edge.

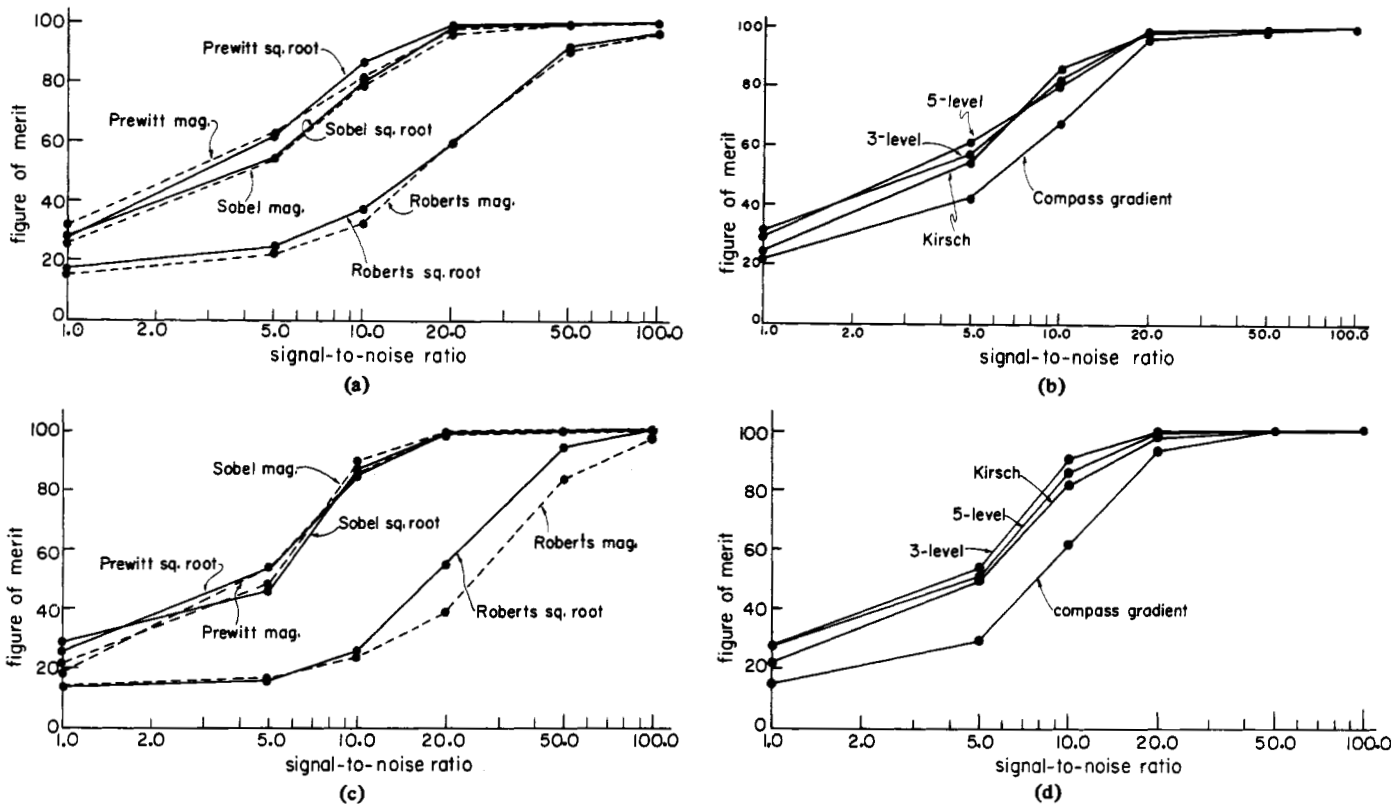

Fig. 13. Figure of merit as a function of signal-to-noise ratio for 2 X 2 and 3 X 3 operators. (a) Differential operators, vertical edge. (b) Template operators, vertical edge. (c) Differential operators, diagonal edge. (d) Template operators, diagonal edge.

Pratt's figure of merit measurement procedure utilizes a square array of pixels with a vertically oriented ramp edge in its center as shown in Fig. 11(a). The edge parameters and noise level can be varied to generate test edges which are then processed by an edge detector to produce binary edge maps. The figure of merit is defined as

$$F = \frac{1}{\max\{I_I, I_A\}} \sum_{i=1}^{I_A} \frac{1}{1 + \alpha d^2(i)} \tag{23}$$

where I_I and I_A are the number of ideal and actual edge points, $d(i)$ is the pixel miss distance of the ith edge detected, and α is a scaling constant chosen to be $\alpha = \frac{1}{9}$ to provide a relative penalty between smeared edges and isolated, but offset, edges.

This technique can be extended to diagonal edges as indicated in Fig. 12. Edge pixels are only counted in a centrally located

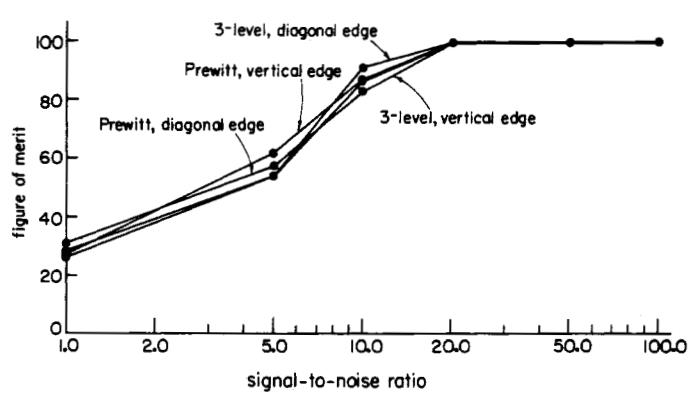

Fig. 14. Figure of merit comparison between differential and template matching operators.

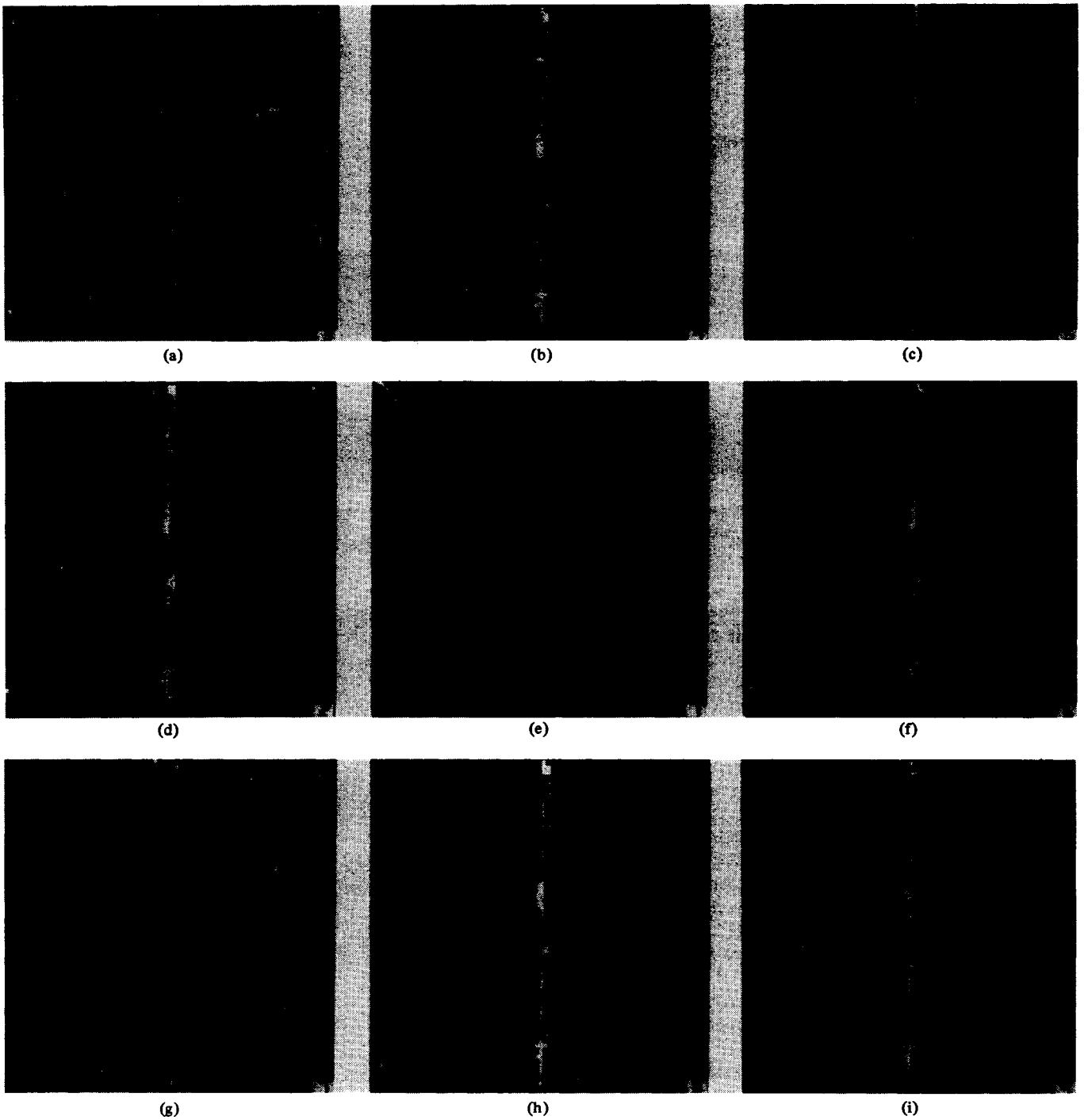

Fig. 15. Edge maps for 2 X 2 and 3 X 3 operators. (a) Prewitt square root vertical edge, SNR = 1, F = 27.5 percent. (b) Prewitt square root vertical edge, SNR = 10, F = 86.5 percent. (c) Prewitt square root vertical edge, SNR = 100, F = 100 percent. (d) Prewitt magnitude vertical edge, SNR = 10, F = 81.5 percent. (e) Prewitt square root diagonal edge, SNR = 10, F = 85.5 percent. (f) Sobel square root vertical edge, SNR = 10, F = 37.6 percent. (h) 3-level vertical edge, SNR = 10, F = 82.4 percent. (i) Kirsch vertical edge, SNR = 10, F = 86.3 percent.

square and miss distances are normalized by the factor $\sqrt{2}$ to account for the discretization distance difference between orthogonal and diagonal paths in an array.

Fig. 13 contains plots of the figure of merit as a function of signal-to-noise ratio for differential and template matching edge detectors. A figure of merit comparison between the best differential and template matching operators is given in Fig. 14. Photographs of detector edge maps corresponding to several of the data points are presented in Fig. 15. The curves indicate that among the class of differential operators, the Prewitt and Sobel operators provide a substantially higher figure of merit than than the Roberts operator. The Prewitt operator exhibits a somewhat larger figure of merit than the Sobel operator for a vertical edge, while for a diagonal edge, their performances are nearly the same. For the template operators, the 3-level, 5-level, and Kirsch operators are clearly superior to the compass gradient operator. The 3-level operator is dominant by a slight margin at all signal-to-noise ratios for diagonal edges, but for vertical edges the relative dominance changes with signal-to-noise ratio. The Prewitt square-root differential operator gives

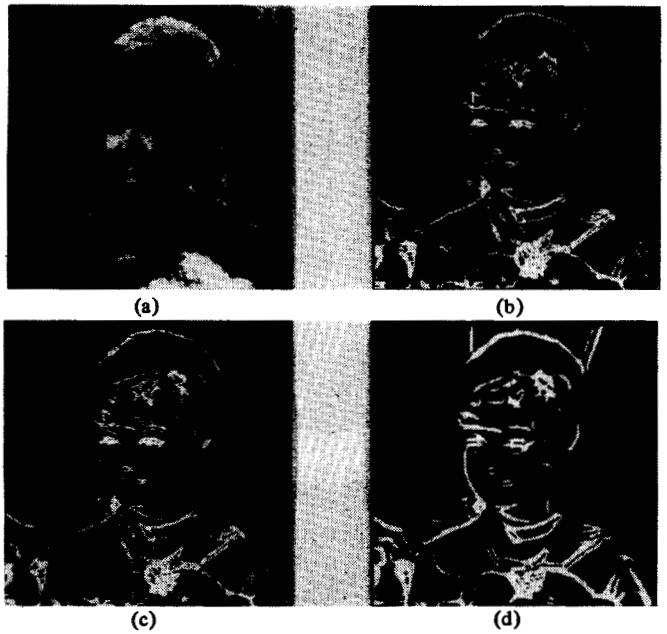

Fig. 16. Examples of edge detection for GIRL picture. (a) Original. (b) 3 X 3 mask, Prewitt differential mask operator. (c) 3 X 3 mask, 3-level template matching operator. (d) 7 X 7 mask, 3-level template matching operator.

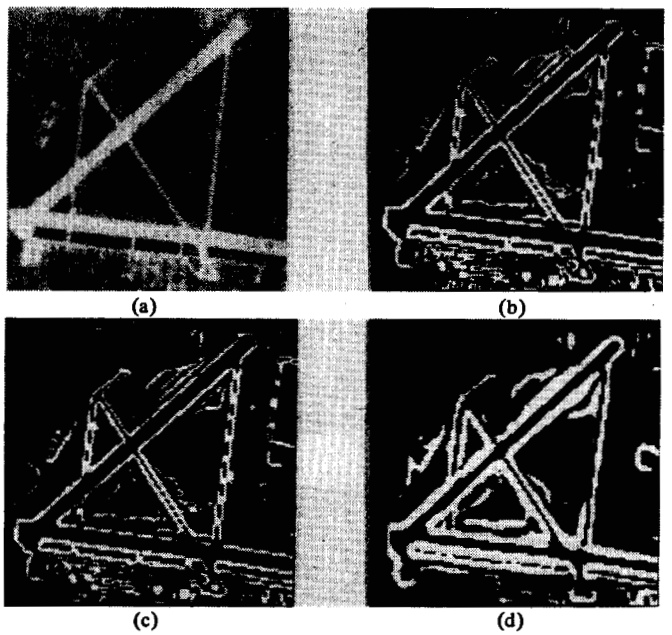

Fig. 17. Examples of edge detection for airport picture. (a) Original. (b) 3 X 3 mask. Prewitt differential mask operator. (c) 3 X 3 mask, 3-level template matching operator. (d) 7 X 7 mask, 3-level template matching operator.

a slightly higher figure of merit than the 3-level template matching operator for vertical edges. For diagonal edges, the reverse is true.

VII. Extended Mask Operators

The design techniques and evaluation methods presented in the previous sections can be applied to larger size masks with a variety of weighting factors. Increasing mask size decreases noise sensitivity because of the inherent noise averaging performed by the operator. However, there is a performance penalty associated with large size masks; displaced edges within the mask contribute to the edge gradient, and therefore, there is an increased potential for false edge detection. The countervailing effects of noise averaging and edge displacement sensitivity can be examined jointly be the figure of merit introduced in Section VI.

Quantitative studies presented in reference [6] indicate that extended mask size edge detectors are superior to 3 X 3 pixel edge detectors at low signal-to-noise ratio. Also, it has been found [6] that amplitude weighting of masks to decrease the influence of pixels distant from the mask center is beneficial in terms of increasing the figure of merit.

VIII. Edge Detection Examples

An important test of the image edge detector design and evaluation procedures presented previously is their value in extracting subjectively relevant object boundaries in real images. Figs. 16 to 18 contain examples of edge detection in three different types of images using the 3 X 3 Prewitt differential operator and the 3 X 3 and 7 X 7 3-level template matching operators. In order to provide a comparison between the three operators, the detector thresholds have been selected so that the number of edges detected is the same for all operators.

There is very little difference between the edge maps of Figs. 16–18 (b) and (c) produced by the 3 X 3 Prewitt and 3-level operators. Both operators have detected most of the object

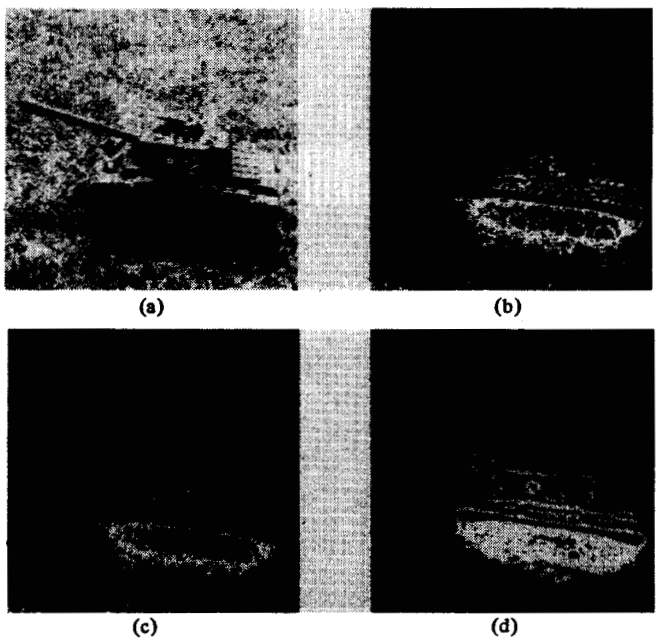

Fig. 18. Examples of edge detection for TANK picture. (a) Original. (b) 3 X 3 mask, Prewitt defferential operator. (c) 3 X 3 mask, 3-level template matching operator. (d) 7 X 7 mask, 3-level template matching operator.

boundary points, and have produced relatively few extraneous edges. The edge broadening effect obtained with the 7 X 7 3-level mask is readily apparent from Figs. 16–18 (d).

IX. Summary

This paper has presented quantitative design and performance evaluation techniques for the enhancement/thresholding class of edge detectors. Two design techniques have been introduced. In one approach, edge detection is viewed as a statistical decision process, and in the other approach, edge detection is considered as a deterministic pattern recognition classification task. It has been shown that the two design approaches are

consistent. The performance evaluation methods developed include: a) deterministic measurement of the edge gradient amplitude; b) comparison of the probabilities of correct and false edge detection; and c) figure of merit computation.

The design and evaluation techniques have been applied to a variety of 2 X 2, 3 X 3, and extended size edge detectors. On the basis of testing, the following conclusions have been formulated.

1) The 3 X 3 differential edge detectors perform appreciably better than the 2 X 2 differential edge detectors.

2) The 3 X 3 Prewitt and Sobel differential edge detectors are the best of the 3 X 3 pixel differential class of edge detectors.

3) The 3-level edge detector is the best of the 3 X 3 pixel template matching class of edge detectors.

4) The 3 X 3 pixel 3-level template matching edge detector and the 3 X 3 pixel Sobel and Prewitt differential edge detectors perform almost equally well as a function of edge orientation and signal-to-noise ratio. It should be noted that differential edge detectors require fewer operations than template edge detectors.

5) Extended mask size edge detectors are superior to 3 X 3 edge detectors at low signal-to-noise ratios.

6) Amplitude weighting of masks of extended size edge detectors is beneficial.

References

[1] W. K. Pratt, *Digital Image Processing*. New York, Wiley-Interscience, 1978.

[2] L. G. Roberts, "Machine perception of three-dimensional solids," in *Optical and Electro-Optical Information Processing*, J. T. Tippett *et al.*, Eds. Cambridge, MA: M.I.T. Press, 1965, pp. 159-197.

[3] J. M. S. Prewitt, "Object enhancement and extraction," in *Picture Processing and Psychopictorics*, B. S. Lipkin and A. Rosenfeld, Eds. New York: Academic Press, 1970.

[4] R. O. Duda and P. E. Hart, *Pattern Classification and Scene Analysis*. New York: Wiley, 1973.

[5] R. Kirsch, "Computer determination of the constituent structure of biological images," *Comput. Biomed. Res.*, vol. 4, no. 3, pp. 315-328, 1971.

[6] I. Abdou, "Quantitative methods of edge detection," Image Processing Institute, Univ. Southern California, Los Angeles, USCIPI Rep. 830, 1973.

[7] K. Fukunaga, *Introduction to Statistical Pattern Recognition*. New York: Academic Press, 1972.

[8] H. C. Andrews, *Introduction to Mathematical Techniques in Pattern Recognition*. New York: Wiley-Interscience, 1972.

[9] Y.-C. Ho and R. L. Kashyap, "An algorithm for linear inequalities and its applications," *IEEE Trans. Electron. Comput.*, vol. EC-14, no. 5, pp. 683-688, Oct. 1965.

[10] J. R. Fram and E. S. Deutsch, "On the evaluation of edge detector schemes and their comparison with human performance," *IEEE Trans. Comput.*, vol. C-24, no. 6, pp. 616-628, June 1975.

[11] E. S. Deutsch and J. R. Fram, "A quantitative study of the orientation bias of some edge detector schemes," *IEEE Trans. Comput.*, vol. C-27, no. 3, pp. 205-213, Mar. 1978.

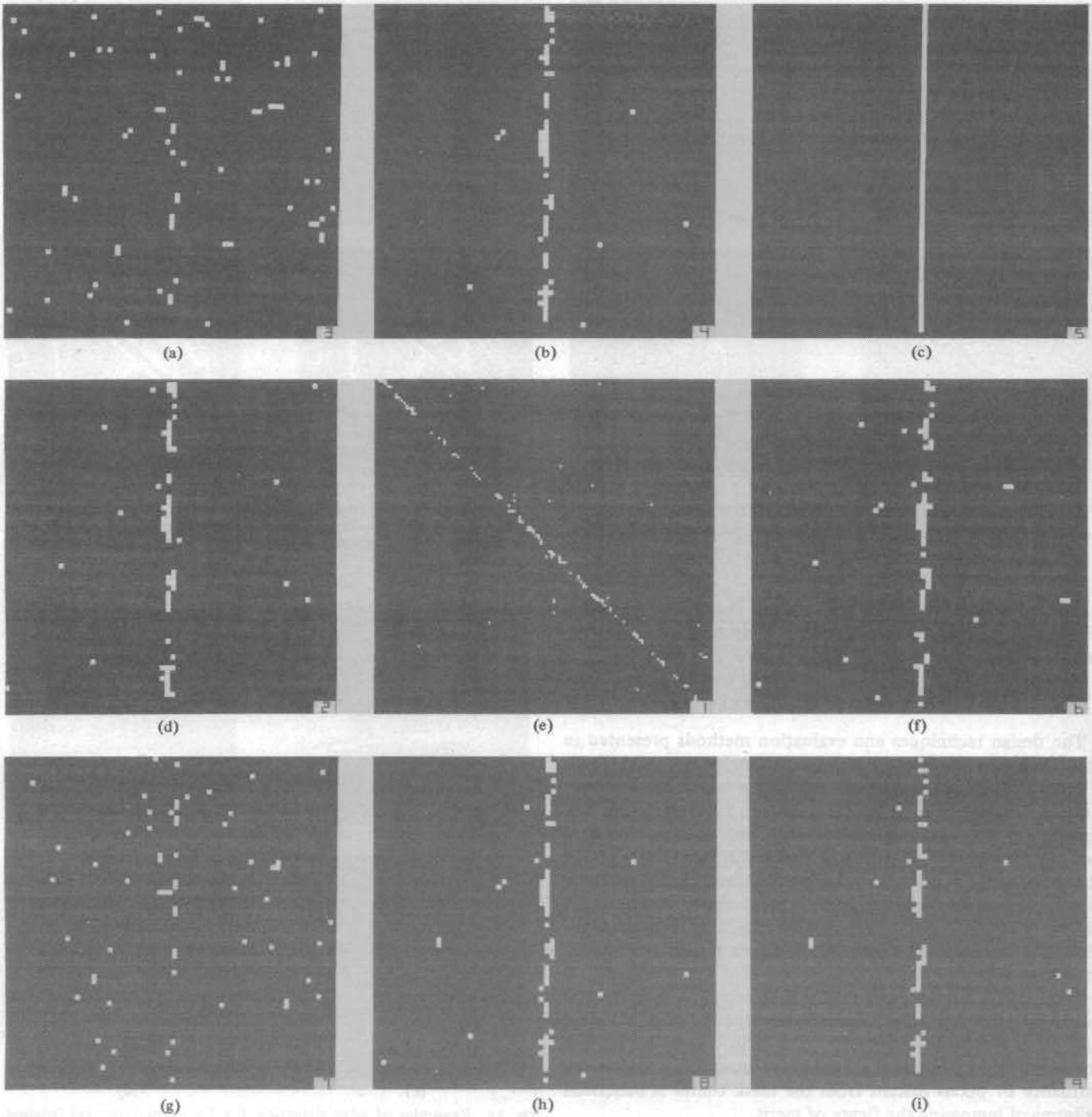

Fig. 15. Edge maps for 2 × 2 and 3 × 3 operators. (a) Prewitt square root vertical edge, SNR = 1, F = 27.5 percent. (b) Prewitt square root vertical edge, SNR = 10, F = 86.5 percent. (c) Prewitt square root vertical edge, SNR = 100, F = 100 percent. (d) Prewitt magnitude vertical edge, SNR = 10, F = 81.5 percent. (e) Prewitt square root diagonal edge, SNR = 10, F = 85.5 percent. (f) Sobel square root vertical edge, SNR = 10, F = 37.6 percent. (h) 3-level vertical edge, SNR = 10, F = 82.4 percent. (i) Kirsch vertical edge, SNR = 10, F = 86.3 percent.

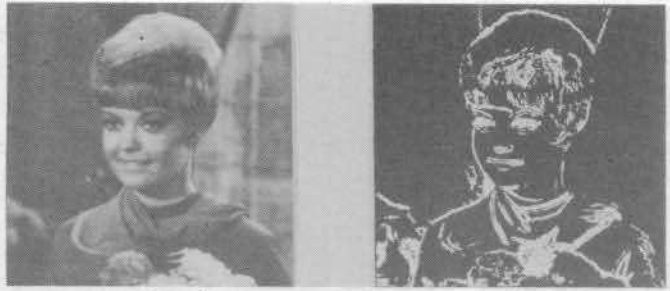

(a) (b)

(c) (d)

Fig. 16. Examples of edge detection for GIRL picture. (a) Original. (b) 3 × 3 mask, Prewitt differential mask operator. (c) 3 × 3 mask, 3-level template matching operator. (d) 7 × 7 mask, 3-level template matching operator.

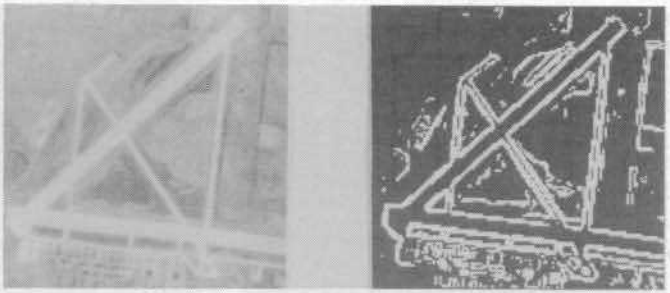

(a) (b)

(c) (d)

Fig. 17. Examples of edge detection for airport picture. (a) Original. (b) 3 × 3 mask. Prewitt differential mask operator. (c) 3 × 3 mask, 3-level template matching operator. (d) 7 × 7 mask, 3-level template matching operator.

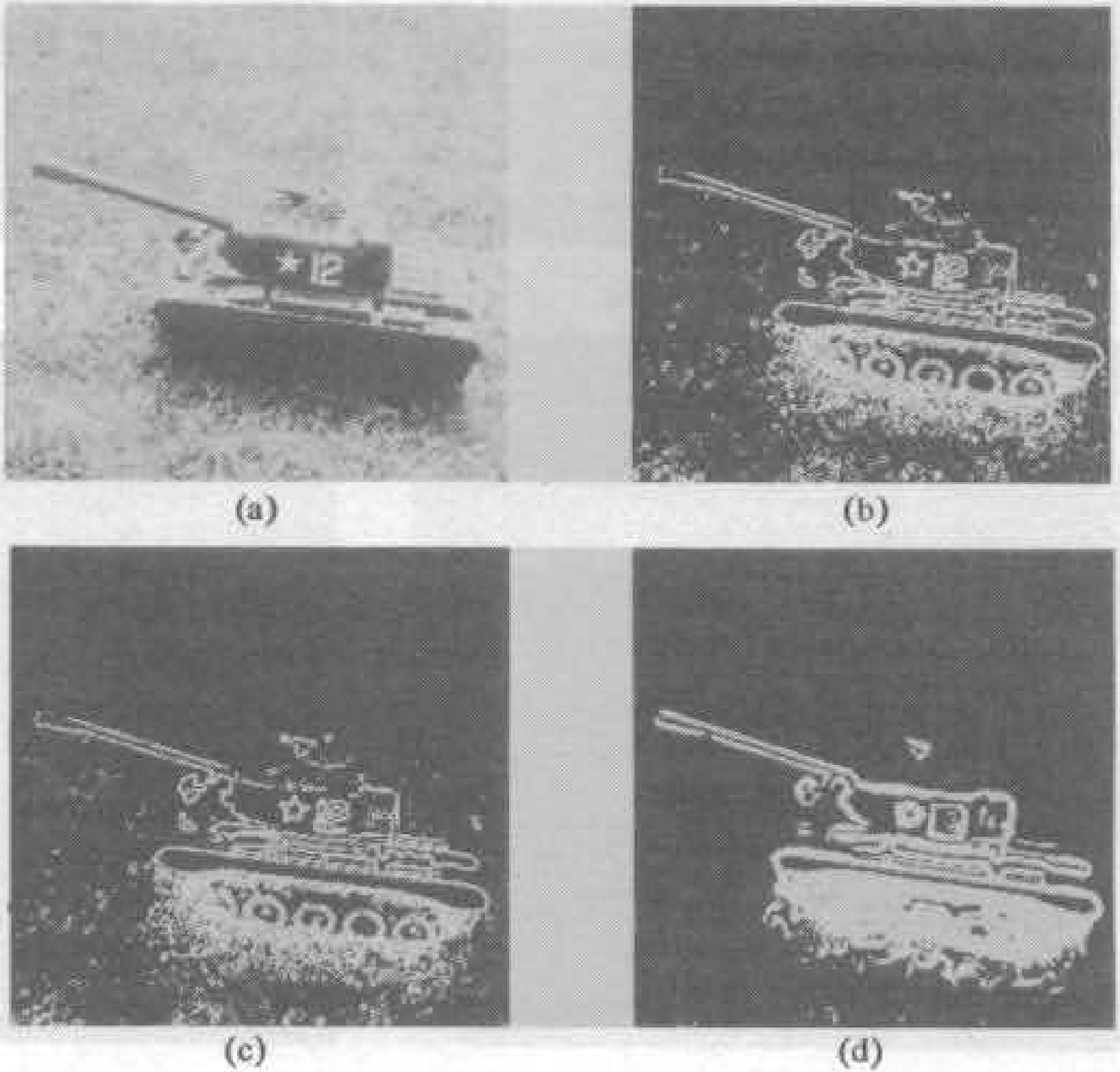

Fig. 18. Examples of edge detection for TANK picture. (a) Original. (b) 3 X 3 mask, Prewitt defferential operator. (c) 3 X 3 mask, 3-level template matching operator. (d) 7 X 7 mask, 3-level template matching operator.